SCIENTIFIC REPORTS

OPEN

SUBJECT AREAS:
GENE EXPRESSION
CLINICAL MICROBIOLOGY
METABOLOMICS

Received
27 August 2013

Accepted
18 November 2013

Published
4 December 2013

Correspondence and requests for materials should be addressed to C.M.S. (cslupsky@ucdavis.edu)

Cross-talk between *E. coli* strains and a human colorectal adenocarcinoma-derived cell line

Xuan He[1], Darya O. Mishchuk[2], Jigna Shah[3], Bart C. Weimer[3] & Carolyn M. Slupsky[1,2]

[1]Department of Nutrition, University of California, Davis, CA 95616-5270, USA, [2]Department of Food Science and Technology, University of California, Davis, CA 95616-5270, USA, [3]School of Veterinary Medicine, University of California, Davis, CA 95616-5270, USA.

Although there is great interest in the specific mechanisms of how gut microbiota modulate the biological processes of the human host, the extent of host-microbe interactions and the bacteria-specific metabolic activities for survival in the co-evolved gastrointestinal environment remain unclear. Here, we demonstrate a comprehensive comparison of the host epithelial response induced by either a pathogenic or commensal strain of *Escherichia coli* using a multi-omics approach. We show that Caco-2 cells incubated with *E. coli* display an activation of defense response genes associated with oxidative stress. Indeed, in the bacteria co-culture system, the host cells experience an altered environment compared with the germ-free system that includes reduced pH, depletion of major energy substrates, and accumulation of fermentation by-products. Measurement of intracellular Caco-2 cell metabolites revealed a significantly increased lactate concentration, as well as changes in TCA cycle intermediates. Our results will lead to a deeper understanding of acute microbial-host interactions.

In the past decade, there has been increasing interest in the study of gut microbial balance and its association with age[1,2], diet[3,4], the immune system[5,6], and metabolic dysfunction[6,7]. Specifically, the energy harvesting capacity of the gut microbiota exerts a strong influence on host metabolism[7,8]. Furthermore, many of the effects of gut microbiota on host metabolism have been accompanied by production of microbe- derived intermediate metabolites and fermentation end-products such as short chain fatty acids (SCFAs), branched chain fatty acids (BCFAs), lactate, ethanol, succinate, and α-keto acids, as well as sulfur compounds, which may further play a role in regulating colonic epithelial cellular proliferation, differentiation, and apoptosis[9].

The internal environment within the gastrointestinal (GI) tract as well as the overall host metabolic signature are largely driven by activities of the well-adapted bacterial communities; thus, these bacteria are viewed as powerful predictors of GI health[10]. Notably, advances in sequencing technologies and high-throughput metagenomics now allow characterization of the microbial community composition in the gut as a functional biomarker for host phenotypes of health and specific diseases[11]. However, the sequence-based approach must be coupled with experiments that define bacterial function to truly understand their role in human health. The integration of genomics and metabolomics promises to provide key insights into the attribution of specific interactions between the host and its microbiota.

Escherichia coli is largely categorized as a commensal bacterium and starts to colonize the human gut with low abundance immediately after birth[12]. Excessively high levels of gram-negative bacteria, including *E. coli*, may be related to changes in intestinal permeability, endotoxaemia, and inflammatory responses associated with obesity and inflammatory bowel disease (IBD)[13]. There is a wide range of *E. coli* genotypes in common strains and serotypes, that includes pathogenic strains that are responsible for infection, and nonpathogenic strains that could be associated with various disease phenotypes. For example, colonization of adherent-invasive *E. coli* was shown to induce local inflammation in individuals with IBD (including Crohn's disease and ulcerative colitis)[14–16], whereas another subset of mucosa-associated *E. coli* was only detected in patients with colon cancer, but not Crohn's disease[17]. Interestingly, alteration of the host metabolic phenotype was also related to the abundance of colonic *E. coli* in several studies[18,19]. For example, elevation of *E. coli* relative abundance in feces has also been associated with excessive weight gain in adolescents[18], and pregnant women[19]. Together, these findings suggest that the colonic *E. coli* strain variation and abundance act to provide a functional complex that interacts with host metabolism and immunity. Thus, understanding the response of the host colonic cells to a single strain of bacteria

in vitro is an important starting point that lays the groundwork to investigate the complex interaction between host and microbes that are common and have very diverse metabolic capacity, such as *E. coli*.

In the present study, a comparative analysis of the comprehensive gene expression profiles and metabolic responses of Caco-2 cells incubated with either *E. coli* K-12 or O157:H7 is followed through high-density oligonucleotide microarrays in combination with ^{1}H NMR metabolomics analysis of both extracellular and intracellular metabolites *in vitro*. The aim of this study is to examine the impact of colonic bacteria on the global gene expression regulation and metabolite levels of the host, and to investigate the molecular mechanics of the *E. coli*/host interaction.

Results

Transcriptional responses of Caco-2 upon interaction with *E. coli* strains. To study the interaction between human intestinal cells and bacterial cells, differentiated Caco-2 cells were incubated with one of two strains of *E. coli* (K-12 or O157:H7) that are non-invasive. Gene expression profiles of the Caco-2 cells were analyzed at three time points: 60, 90, and 120 minutes after co-culture, and compared with the controls in the monoculture. Over 120 minutes of incubation time, Caco-2 cells underwent a strain-specific response to *E. coli*, with more Caco-2 genes that were repressed compared with induced genes in both treatments (Fig. 1, Supplementary Table S1 online). Affected genes included those encoding ion channels, plasma membrane transporters (Table 1), pro-inflammatory mediators, and proto-oncogenes (Table 2, see Supplementary Table S1 online for the complete gene list). Genes that were repressed included transporters for simple sugars and amino acids, such as *SLC7A1*. These transporter genes share a wide range of biological functions, and repression of their expression suggests complex modifications of Caco-2 metabolic activity in response to exposure to *E. coli*. Furthermore, the changes in expression profiles of these genes were observed to be exposure time-dependent, with changes occurring as early as 60 min, suggesting the effect of *E. coli* on host ion channel and plasma membrane transporters occurred quickly after bacterial association, and this may lead to metabolic impact long after initial exposure (Table 1).

Amongst all of the induced genes, many were annotated as pro-inflammatory cytokines/chemokines (*CXCL1*, *CXCL2*, *CXCL3*, and *IL1A*). Interestingly, the expression level of *TNF-α* remained constant in Caco-2 cells while co-culturing with either of the *E. coli* strains; however, alpha-induced protein 3 gene (*TNFAIP3*, also known as *A20*) was induced, and TNF receptor-associated factor 3 (*TRAF3*) was repressed in both bacterial conditions as compared to the germ-free control. Several proto-oncogenes were also induced, including *SOD2*, *JUN* and *FOS* (Table 2).

Metabolic responses of Caco-2 upon interaction with *E. coli* strains. A comparison of 41 extracellular metabolites measured by ^{1}H NMR spectroscopy after 60 min of incubation of Caco-2 cells with media or with *E. coli* K-12 revealed substantial differences when compared with the starting medium (Fig. 2a). Although a clear separation in the first Principal Component (PC1) was observed between the co-culture and *E. coli* K-12 alone (Fig. 2b), the difference between the metabolic profiles and either the starting medium or Caco-2 grown without bacteria, suggests that the co-metabolism of the host and microbe *in vitro* was largely driven by the bacterial metabolic capability.

To further characterize the impact of *E. coli* on the extracellular metabolic profile, and the subsequent change with time, repeated measure models for both *E. coli* strains (K-12 and O157:H7), Caco-2 cells, and the two co-culture systems at 60, 90 and 120 min were investigated. Utilization of nutrients from the cell culture medium by either *E. coli* strains led to depletion of major energy substrates, such as glucose and glutamine, and production of SCFAs, succinate, formate, ethanol and lactate (multiple repeated measures ANOVAs, FDR corrected p-value < 0.05 for comparisons between Caco-2 control and Caco2-*E. coli* K-12 co-culture, Fig. 3). Generation of acetate accounted for >99% of the total SCFA concentration in the extracellular medium. Furthermore, the extracellular pH decreased (repeated measures ANOVA, p-value < 0.0001, Fig. 4a) reflecting the accumulation of organic acids. Interestingly, similar extracellular metabolic patterns for both *E. coli* K-12 and O157:H7 were observed with the exception of a few metabolites. For example, propionate was only detected in *E. coli* K-12 broth as well as the associated co-culture with Caco-2 cells. Production of acetate, ethanol, formate, lactate and succinate, as well as the utilization of glucose and glutamate, was largely accelerated in the *E. coli* K-12 control and the associated co-culture environment compared with the *E. coli* O157:H7 system. The accumulation of fumarate in the supernatant was also strain specific, as the *E. coli* O157:H7 monoculture produced more than the *E. coli* K-12 monoculture, and the same trend was observed when comparing the associated cocultures (repeated measures ANOVA, FDR corrected p-value < 0.05 for comparisons between *E. coli* K-12 controls and *E. coli* O157:H7 controls as well as the comparisons on the associated co-culture conditions, Fig. 3).

To monitor the influence of *E. coli* K-12 exposure on Caco-2 intracellular metabolites, Caco-2 metabolites in both the monoculture and co-culture were measured at 60 min. In comparison to the monoculture condition, 22 out of 48 intracellular metabolites were significantly different at 60 min (multiple t-tests, FDR corrected p-value < 0.05, Supplementary Table S3). Lactate concentration increased 1.8-fold in the co-culture (multiple t-tests, p-value < 0.05, Fig. 5a), which further explained the reduction of intracellular

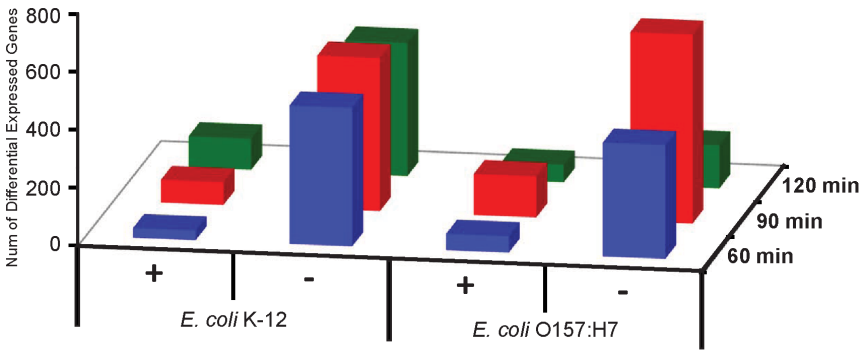

Figure 1 | Summary of the interaction between Caco-2 cells and each of two *E. coli* strains (K-12 or O157:H7) reflected in global transcriptional changes. Of the 21,000 genes that were screened, the numbers of up (+) and down (−) differentially expressed genes in Caco-2 cells at each time point are shown.

Table 1 | *E. coli* K-12 and O157:H7 modified gene expression of ion channel and plasma membrane transporters in Caco-2 cells at 60, 90 and 120 min

Coculture, time	Symbol	Mean Fold Change	Entrez Gene Name	Type (s)	Regulates
k-12, 60 min	*CLCN4*	−1.204	Chloride channel 4	ion channel	Chloride
	SLC7A1	−1.214	Solute carrier family 7 (cationic amino acid transporter, y+ system), member 1	transporter	arginine, basic amino acid, amino acids, L-lysine, L-amino acid, L-ornithine, L-arginine, reporter mRNA, nitric oxide
	STXBP3	−1.224	Syntaxin binding protein 3	transporter	STX4, Insulin, INS, D-glucose, RAB4A, VAMP2, SLC2A4, IL1RN, SNAP23
k-12, 90 min	*CACNA1D*	−1.223	Calcium channel, voltage-dependent, L type, alpha 1D subunit	ion channel	calcium, FOS, Ca2+, Il12, RYR2, KCNJ2, APOE, Ins1, CACNA1C, BDNF, cholesterol, glycine, GABA, L-glutamic acid, Ryr
	SLC22A11	−1.294	Solute carrier family 22 (organic anion/urate transporter), member 11	transporter	organic anion, ketoprofen, indomethacin, aspirin, salicylic acid, ibuprofen
	TRPV1	−1.244	Transient receptor potential cation channel, subfamily V, member 1	ion channel	Ca2+, calcium, TRPV1, gastric acid, L-glutamic acid, peptide, cation, lipid, nitrite, GFAP, FOS, HLA-DQB1 (includes others), CALCB, PTGS2, nitric oxide
k-12, 120 min	*SLC10A4*	−1.398	Solute carrier family 10 (sodium/bile acid cotransporter family), member 4	transporter	---
	SLC20A1	1.222	Solute carrier family 20 (phosphate transporter), member 1	transporter	phosphate, Na+, GH1
	SLC7A1	−1.215	Solute carrier family 7 (cationic amino acid transporter, y+ system), member 1	transporter	arginine, basic amino acid, amino acids, L-lysine, L-amino acid, L-ornithine, L-arginine, reporter mRNA, nitric oxide
O157:H7, 60 min	*SLC2A10*	−1.293	Solute carrier family 2 (facilitated glucose transporter), member 10	transporter	D-glucose
	SLC7A1	−1.222	Solute carrier family 7 (cationic amino acid transporter, y+ system), member 1	transporter	arginine, basic amino acid, amino acids, L-lysine, L-amino acid, L-ornithine, L-arginine, reporter mRNA, nitric oxide
O157:H7, 90 min	*ABCC3*	−1.254	ATP-binding cassette, sub-family C (CFTR/MRP), member 3	transporter	bile salt, organic anion, bile acid, taurocholic acid, etoposide, etoposide glucuronide, methotrexate, glycocholic acid, etc
	CACNA1D	−1.267	Calcium channel, voltage-dependent, L type, alpha 1D subunit	ion channel	calcium, FOS, Ca2+, Il12, RYR2, KCNJ2, APOE, Ins1, CACNA1C, BDNF, cholesterol, glycine, GABA, L-glutamic acid, Ryr
	GRIN2D	−1.262	Glutamate receptor, ionotropic, N-methyl D-aspartate 2D	ion channel	Ca2+, calcium, GRIN1, GRIN2D, NMDA Receptor, NOS1, CASP3, Ras, L-glutamic acid, Creb, AKT1, PTGS2, DOPAMINE D1 RECEPTOR, CASP9, MAPK14
	KCNC4	−1.319	Potassium voltage-gated channel, Shaw-related subfamily, member 4	ion channel	Neurotransmitter
	KCNJ2	−1.286	Potassium inwardly-rectifying channel, subfamily J, member 2	ion channel	MYEF2, MYOG, KCNJ2, FOS
	SLC39A14	−1.230	Solute carrier family 39 (zinc transporter), member 14	transporter	heavy metal, Zn2+, metal
	SLC5A3	1.214	Solute carrier family 5 (sodium/myo-inositol cotransporter), member 3	transporter	myo-inositol, D-glucose

Gene function annotation is characterized based on the IPA Knowledge Base.

pH (monoculture: 7.05 ± 0.04; co-culture: 6.80 ± 0.03, t-test, p-value = 0.001, Fig. 4b). The intracellular concentration of amino acids, such as glutamine (Fig. 5b), glycine (Fig. 5c), threonine, and tryptophan were lower in the co-culture (multiple t-tests, FDR corrected p-value < 0.05, Supplementary Table S3); however, branched chain amino acids (BCAAs) such as isoleucine, leucine and valine were significantly higher when compared with the control (Fig. 5d). Intracellular glucose (Fig. 5e), aspartate (Fig. 5f) and uridine (Fig. 5g) concentrations were significantly lower in the co-culture, whereas the TCA cycle intermediates, succinate (Fig 5h) and fumarate (Fig 5i), were higher and lower, respectively, in the K-12 co-culture. Although the concentration of α-ketoglutarate was higher in the supernatant during K-12 exposure (multiple repeated measures ANOVAs, FDR corrected p-value < 0.05 for comparisons between Caco-2 control and Caco2-*E. coli* K-12 co-culture, Fig. 3), it was not detected in the intracellular concentration. Overall, these intracellular measurements are in agreement with the extracellular measurements except in the case of fumarate. Generally, the metabolic responses of Caco-2 upon interaction with *E. coli* are in agreement with the gene expression responses of Caco-2 cells with respect to the *E. coli* induced suppression of the glucose and amino acid transporter genes.

Discussion

In the present study, it was shown that the profile of extracellular metabolites in a Caco2-*E. coli* co-culture was primarily determined

Table 2 | Top functional genes in Caco-2 cells associated with host-bacterial interaction

	Mean Fold Change							
	Caco-2 incubated with *E. coli* K-12			Caco-2 incubated with *E. coli* O157:H7				
Symbol	60 min	90 min	120 min	60 min	90 min	120 min	Location	Type(s)
CXCL1	1.433	1.456	1.473	1.573	1.679	1.650	Extracellular Space	cytokine
CXCL2	1.738	1.885	1.848	1.877	2.026	1.953	Extracellular Space	cytokine
CXCL3	1.415	1.424	1.486	1.531	1.613	1.646	Extracellular Space	cytokine
GADD45B	1.358	1.400	1.532	1.242	1.374	1.474	Cytoplasm	other
JUN	1.297	1.459	1.517	1.312	1.504	1.583	Nucleus	transcription regulator
MED17	−1.292	−1.254	−1.309	−1.282	−1.308	−1.332	Nucleus	transcription regulator
MYL12A	1.214	1.391	1.473	1.218	1.475	1.501	unknown	other
PPIA	−1.684	−1.419	−1.480	−1.450	−1.737	−1.498	Cytoplasm	enzyme
RCAN1	1.581	1.503	1.515	1.648	1.623	1.638	Nucleus	transcription regulator
SOD2	2.404	2.714	2.587	2.352	3.170	3.054	Cytoplasm	enzyme
GTF2A2	−1.346	−1.306	−1.329	−1.266	−1.275		Nucleus	transcription regulator
TNFAIP3	1.215	--	1.254	1.297	1.239	1.407	Nucleus	enzyme
TRIM25	−1.230	−1.293	−1.282	--	−1.262	−1.331	Cytoplasm	transcription regulator
HGD	--	1.241	1.206	--	1.241	1.328	Cytoplasm	enzyme
FOS	--	1.396	1.444	--	1.387	1.418	Nucleus	transcription regulator
FARSB	--	−1.201	−1.243	--	−1.324	−1.223	Cytoplasm	enzyme
CDK5R1	--	−1.382	−1.468	--	−1.340	−1.642	Nucleus	kinase
CNOT7	−1.205	−1.254	--	--	−1.251	−1.309	Nucleus	transcription regulator
HDAC4	−1.290	−1.258	--	−1.215	−1.245	--	Nucleus	transcription regulator
HIPK2	−1.262	--	--	−1.217	−1.278	−1.216	Nucleus	kinase
GNAS	−1.211	−1.236	−1.275	--	--	−1.223	Plasma Membrane	enzyme
KLF4	−1.289	−1.291	−1.328	--	--	−1.243	Nucleus	transcription regulator
USP42	−1.240	−1.200	−1.250	−1.254	--	--	unknown	peptidase
VAPA	−1.349	−1.375	−1.373	−1.323	--	--	Plasma Membrane	other
MED13	−1.325	−1.365	--	−1.219	−1.291	--	Nucleus	transcription regulator
NFIC	−1.218	−1.290	--	−1.255	−1.263	--	Nucleus	transcription regulator
SKI	−1.219	−1.213	--	−1.270	−1.206	--	Nucleus	transcription regulator
SYNJ2	−1.242	−1.432	--	−1.204	−1.451	--	Cytoplasm	phosphatase
ACVR1B	−1.208	−1.204	--	−1.212	--	--	Plasma Membrane	kinase
IL1A	−1.211	−1.277	--	−1.340	--	--	Extracellular Space	cytokine
IGF1R	−1.247	−1.226	--	−1.251	--	--	Plasma Membrane	transmembrane receptor
TRAF3	−1.227	−1.213	--	--	−1.209	--	Cytoplasm	other
ADRB1	--	−1.326	--	--	−1.266	−1.269	Plasma Membrane	G-protein coupled receptor
TNS1	--	−1.212	--	−1.235	−1.228	--	Plasma Membrane	other
BTG2	--	--	1.224	--	1.345	1.361	Nucleus	transcription regulator
MAVS	--	--	−1.223	--	−1.203	−1.232	Cytoplasm	other
CCL20	--	--	--	1.445	1.554	1.375	Extracellular Space	cytokine
IL8	--	--	--	1.482	1.614	1.637	Extracellular Space	cytokine
EIF3B	--	−1.326	−1.222	--	--	−1.351	Cytoplasm	translation regulator
SOS1	--	−1.211	−1.421	--	--	−1.401	Cytoplasm	other
HSD3B1	--	−1.322	−1.283	--	−1.305	--	Cytoplasm	enzyme
NOC2L	--	−1.308	−1.235	--	−1.501	--	Nucleus	transcription regulator
ELAVL1	−1.227	--	--	−1.202	−1.240	--	Cytoplasm	other
TLK1	−1.227	--	--	−1.219	−1.258	--	Cytoplasm	kinase
RDH13	−1.208	--	--	−1.236	−1.229	--	Cytoplasm	enzyme
SLC7A1	−1.214	--	−1.215	−1.222	--	--	Plasma Membrane	transporter
HIST1H1E	1.339	1.238	1.427	--	--	--	Nucleus	other
HS3ST1	--	--	−1.242	−1.212	--	−1.297	Cytoplasm	enzyme

by the bacteria. Furthermore, co-culture of Caco-2 cells with either *E. coli* K-12 or *E. coli* O157:H7 resulted in similar extracellular metabolic patterns with the exception of propionate and a few other metabolites that differed by the magnitude of change (including the production of acetate, ethanol, formate, succinate and lactate as well as the utilization of glucose and glutamate, Fig. 3). Specifically, the capability of producing propionate by *E. coli* K-12, but not pathogenic *E. coli* O157:H7, is particularly interesting as propionate has been linked to reduced inflammation in patients with IBD[20]. The gene expression data revealed that introduction of bacteria to host epithelial cells induced an acute inflammatory response. For example, induction of the Jun/Fos family of the activation protein 1 (Ap-1) complex was observed (Table 2), which may be linked with a rapid induction of a wide range of cytokines that initiates stress-response pathways that protect against oxidative damage by increased production of reactive oxygen species (ROS), which is further confirmed by SOD induction. The Ap-1 transcriptional factor as the downstream target of signaling cascades of the Mitogen-activated protein kinases (MAPKs, including ERKs, JNKs and p38s), may further lead to cell type-specific biological responses including control of cell cycle, cell survival, death, and apoptosis[21]. Moreover, the enhanced *GADD45B* gene response to environmental stress by activation of the p38/JNK pathway could follow the stressful growth arrest condition and induce cell apoptosis[22]. Taken together, we

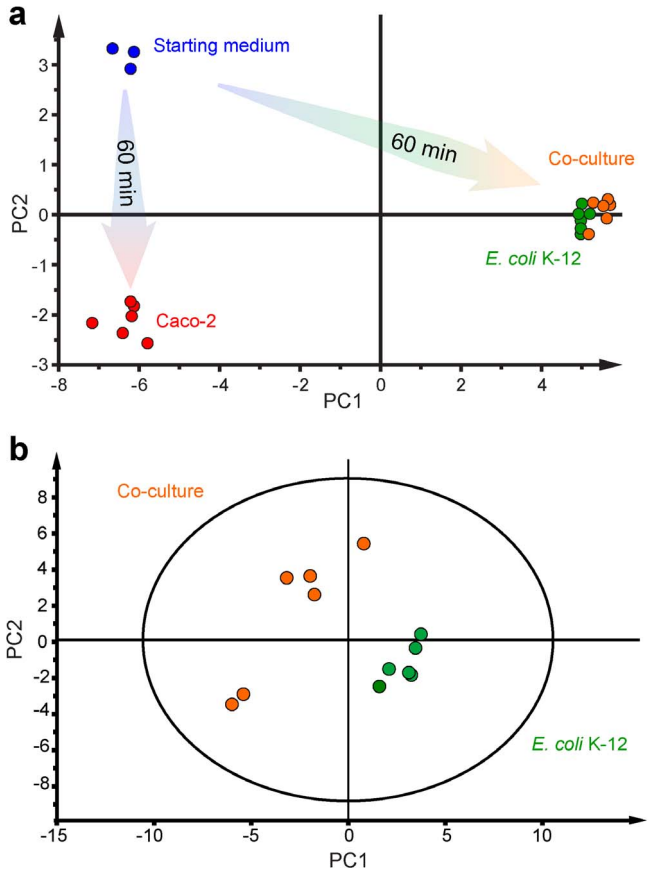

Figure 2 | Principal Component Analysis (PCA) of extracellular metabolites determined by ^{1}H NMR data. (a). The PCA scores plot is based on a full resolution NMR data set consisting of six replicates of Caco-2 cells, *E. coli* K-12 cells, and Caco2-*E. coli* co-culture, four replicates of starting medium, and a total of 41 measured metabolites (goodness of fit, $R^2 = 0.952$; prediction reliability, $Q^2 = 0.932$). (b). The PCA scores plot illustrates a separation between the extracellular metabolic profiles of *E. coli* K-12 cells and Caco2-*E. coli* co-culture (goodness of fit, $R^2 = 0.662$; prediction reliability, $Q^2 = 0.286$).

speculate that the bacteria-induced inflammatory responses in Caco-2 cells may initiate oxidative stress, which potentially leads to epithelial cell damage if persistently exposed to the microbes *in vitro*.

Interestingly, induction of *SOD2* that encodes for manganese superoxide dismutase (SOD) potentially protects injured tissues from excess production of superoxide radicals in the mitochondria[23]. The activation of *SOD2* in both of the co-cultures suggests activation of a defense response against injury from oxygen radicals, and the need for the proliferation and repopulation of damaged or killed cells. These results indicate that Caco-2 cells might be subjected to significant oxidative stress and inflammation during incubation with *E. coli*.

A similar trend in inflammatory response has been reported in various animal models. For example, after oral introduction of fecal bacteria to germ-free mice, Sydora *et al*[24]. reported an imbalance of cytokines, including interferon gamma (IFN-γ), tumor necrosis factor alpha (TNF-α) and interleukin 17 (IL-17) at day 3 of exposure to the microbes, as well as an increase of colonic and caecal histopathological injury score at day 7. Similarly, the gene expression profiles of colonic epithelial cells isolated from germ-free mice inoculated with fecal material revealed an induction of genes associated with apoptosis and the immune response, and repression of genes participating in extracellular oxidant defense and cellular metabolism compared with germ-free mice[25]. Findings from this study suggest that the changes in expression of Caco-2 genes associated with immune activation in the co-culture condition are independent of the acute shortage of energy substrates at later experimental time points.

Indeed, the nature of the interactions with epithelial cells is different between *E. coli* K-12 and *E. coli* O157:H7. For example, *E. coli* K-12, like most other commensal E. coli strains, tends to accumulate in the mucus layer, and thus lack the direct interaction with epithelial cells. However, *E. coli* O157:H7, also known as Enterohemorrhagic *Escherichia coli* (EHEC), is able to swim through the mucus layer, attach intimately to the enterocytes, inject bacterial Esps (EPEC-secreted proteins) inside the eukaryotic cells via type III secretion system[26], to produce attaching and effacing lesions on the intestinal epithelial cells[27]. However, the direct contact of *E. coli* K-12 and host cells, which usually do not occur *in vivo*, was induced in our study by applying centrifugal force to physically enhance bacterial adhesion. Furthermore, Caco-2 cells do not produce mucus like intestinal cells do *in vivo*; therefore, both *E. coli* strains have the ability to interact directly with the host cell. These results together could provide an explanation for the similarities between *E. coli* K-12 and *E. coli* O157:H7 in both metabolic change and inflammatory response that was captured in the Caco-2 gene expression profile.

In a culture-based environment, bacterial activities tend to become competitive with host cells for nutrients and energy. For example, growth of *E. coli* by itself and in the co-culture environment was largely stimulated by the medium rich in glutamine and glucose. Bacterial utilization of glucose to produce various intermediate metabolites and mixed acid end-products reduces the energy available to the host cells. Noticeably, the key issue in fermentation is the recycling of reducing NADH to regenerate the oxidized form, NAD^+, to maintain glycolytic flux for ATP production. *E. coli* could achieve this by replacing the reducing equivalents onto partially oxidized metabolic intermediates[28], which in turn explains the accumulation of lactate, succinate, formate, and ethanol in the supernatant (Fig. 3). Furthermore, the conversion from pyruvate to acetate is energetically favorable (oxidation state = 0) which allows generation of energy in the form of ATP[28,29]. *E. coli* K-12 and the associated co-culture experiments utilized slightly more glucose in the supernatant compared with *E. coli* O157:H7, and subsequently produced more acetate over time (repeated measures ANOVA, FDR corrected p-value $<$ 0.05 for comparison between *E. coli* K-12 controls and *E. coli* O157:H7 controls as well as the comparison on the associated co-culture conditions, Fig. 3). The accumulation of SCFAs (predominantly acetate), in the form of weak acids, explains the decrease of pH over time (repeated measures ANOVA, p-value $<$ 0.0001, Fig. 4a). In addition, generation of fermentation products is pH dependent; as pH drops, cells produce more lactate instead of acetate and formate[28]. Together, these data explain the slightly increased production of lactate in *E. coli* K-12 and the associated co-culture system compared with *E. coli* O157:H7.

In Caco-2 cells, the decrease in intracellular glucose (Fig. 5e) with co-culture could be associated with the depletion of glucose and glutamine in the extracellular supernatant (multiple repeated measures ANOVAs, FDR corrected p-value $<$ 0.05 for comparisons between Caco-2 control and Caco2-*E. coli* K-12 co-culture, Fig. 3). To the best of our knowledge, the extracellular glucose concentration should be enough to maintain cellular activity for 60 min. Interestingly, intracellular concentrations of BCAAs significantly increased in Caco-2 cells after 60 min exposure to *E. coli* K-12 (Fig. 5d). The source of the BCAAs could either be due to an alteration of the cellular permeability as an effect of bacterial adhesion, or amino acid production by Caco-2 cells during carbohydrate starvation conditions[30–34], or an innate inflammatory response. In any event, the increased intracellular BCAAs may provide a metabolic source to maintain elevated glutamine levels, and thus metabolic activity within the Caco-2 cells. Furthermore, it is important to note that the measured intracellular metabolites from the co-culture could

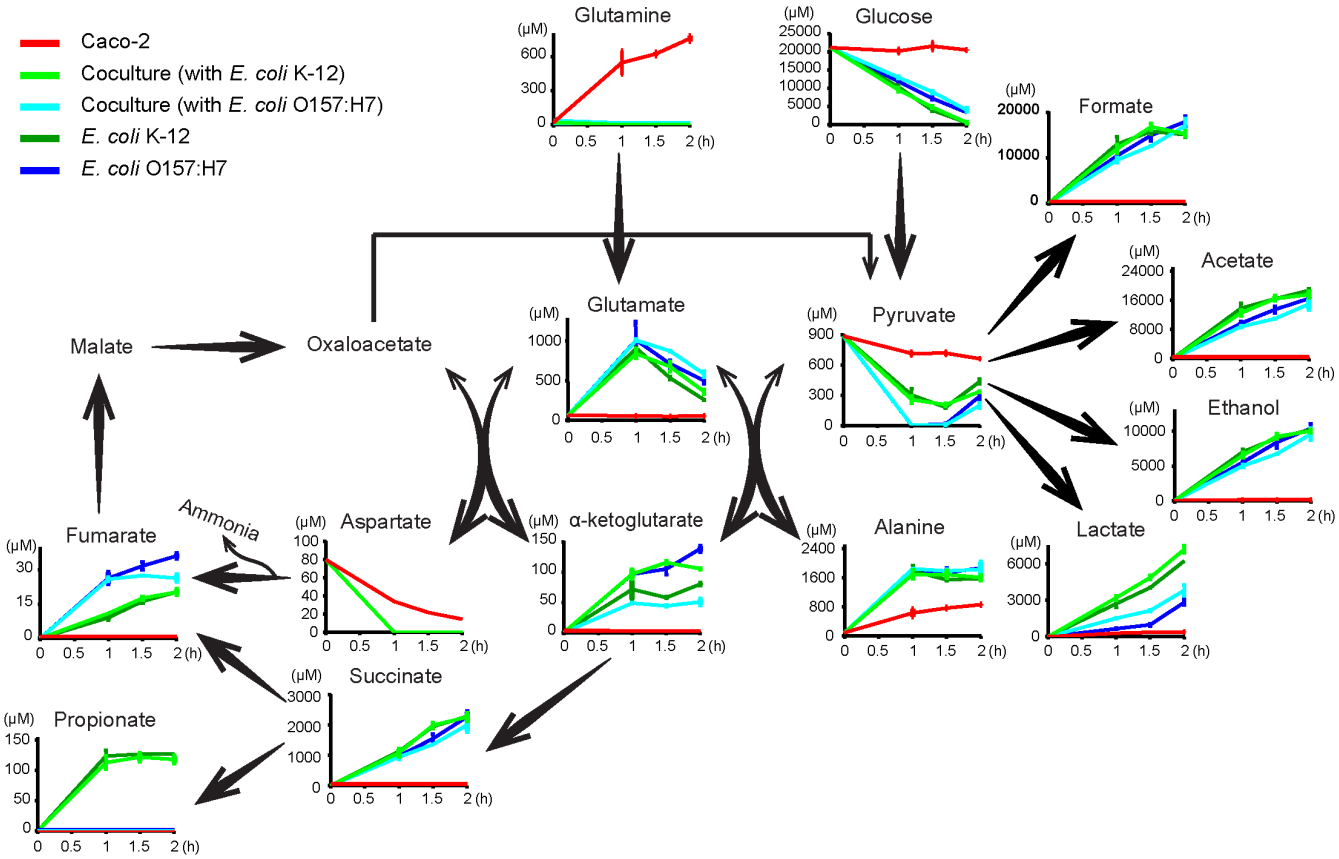

Figure 3 | Dynamic changes of extracellular metabolite concentrations. Time series metabolite data measured at 60, 90 and 120 min of the supernatant collected from cultures of: Caco-2 cells (red), *E. coli* K-12 (dark green), *E. coli* O157:H7(dark blue), Caco-2 cells co-cultured with *E. coli* K-12 (light green), and Caco-2 cells co-cultured with *E. coli* O157:H7(cyan). All data are displayed as mean ± SEM and expressed relative to the 0 min value which corresponds to the concentration of metabolites in the starting culture medium. Two biological replicates were performed for each treatment.

also reflect bacterial contamination due to an inability to completely remove bacteria during the washing process. However, since no specific bacterially derived metabolites were detected in the intracellular extraction, and significantly lower concentrations of microbial end-products (such as acetate, Supplementary Table S3 online) were observed in co-cultured Caco-2 relative to Caco-2 in monoculture, suggests that bacterial contamination was negligible.

Aspartate, glutamine and glycine are key metabolites involved in synthesis of purines and pyrimidines. We observed a significant decrease of these metabolites in the Caco-2 cytosol with co-culture (Fig. 5b,c,f). Furthermore, intracellular uridine and glycine concentrations were reduced with bacterial exposure (Fig. 5g). We hypothesize that the decreased uridine was due to the observed low level of glycine, and thus an alteration in *de novo* synthesis. Of further inter-

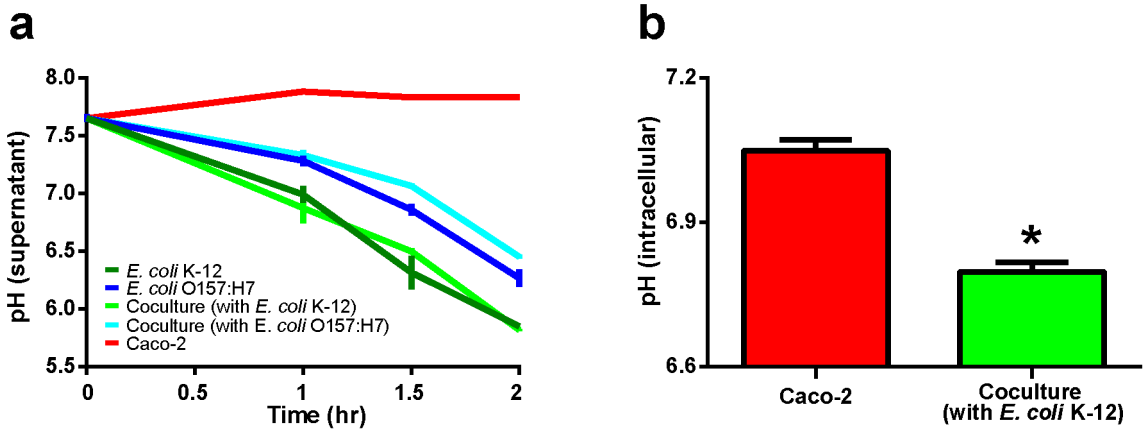

Figure 4 | Comparison of pH between co-cultures and monocultures. (a) Time series measurements of extracellular pH indicate that bacteria induced acidification of the supernatant over time. A decrease of pH over time of the *E. coli* K-12 (green) and its corresponding co-culture system with Caco-2 (light green) is faster than *E. coli* O157:H7 (blue) and its corresponding co-culture system (cyan). Two biological replicates were performed for each treatment. (b) Intracellular pH of Caco-2 cells alone (red) versus Caco-2 incubated with *E. coli* K-12 (green). Three biological replicates were performed for each treatment. Result is displayed as mean ± SEM. Significant differences were computed by student's t-test and identified with *p = 0.001.

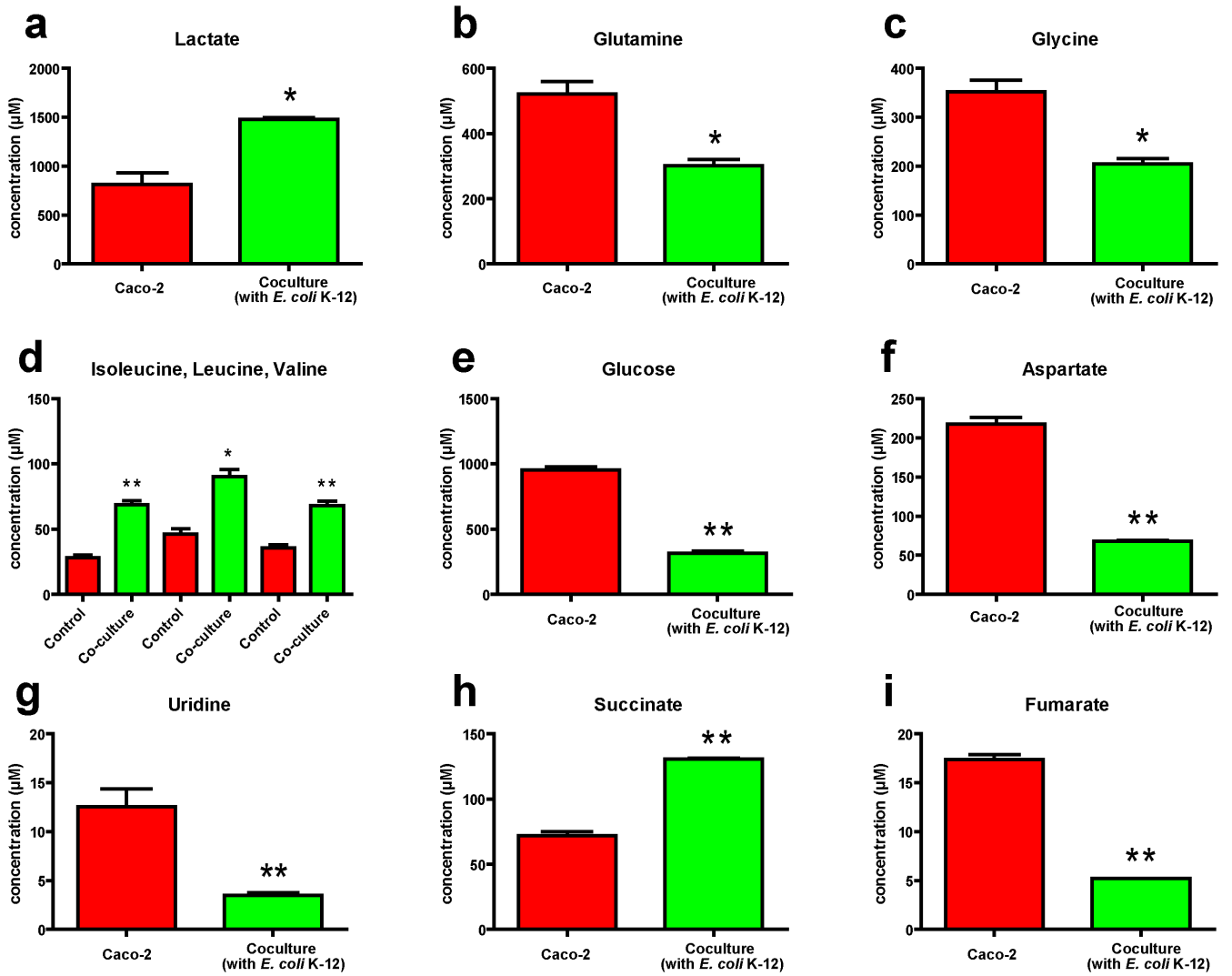

Figure 5 | Intracellular responses of Caco-2 cells to E. *coli* K-12 after 60 mins. (a) lactate, (b) glutamine, (c) glycine, (d) isoleucine, leucine, valine, (e) glucose, (f) aspartate, (g) uridine, (h) succinate, (i) fumarate. Results are displayed as mean ± SEM. Significant differences were adjusted by FDR after multiple comparisons by student's t-test and are identified with *$p < 0.05$, **$p < 0.005$. Three replicates were averaged for each condition. The complete summary data for all the identified intracellular metabolites are available online (Supplementary table S3).

est, succinate (Fig. 5h) increased, while fumarate (Fig. 5i) decreased during co-culture, indicating that succinate dehydrogenase function could be insufficient. Indeed, in addition to α-ketoglutarate, both succinate and fumarate are major entry/exit points to the TCA cycle to produce glyoxylates. The fact that no difference in concentration of α-ketoglutarate in co-culture compared to the monoculture is interesting, particularly since α-ketoglutarate is a precursor for glutamate/glutamine. However, all keto-acids are pre-cursors to organic acids during carbohydrate starvation in bacteria found in the gut[30–34]. Glutamine is noteworthy because it is one of the primary energy sources of the colorectal epithelium[22,35] via deamination to glutamate by mitochondrial phosphate-dependent glutaminase to generate α-ketoglutarate and maintain the TCA cycle. This metabolic route is also found in bacteria. Glutamine metabolism is essential for utilization of its carbon chain, amino group, and amide nitrogen to support a number of metabolic pathways such as synthesis of other amino acids (e.g. arginine, proline, and ornithine), as well as purines, pyrimidines, and amino sugars[35].

The metabolism of tumor cells is characterized by a high rate of glycolysis associated with a lowered pyruvate oxidation rate, increased production of lactate, and decreased activities of the malate-aspartate shuttles[36]. The majority of pyruvate is converted to lactate via lactate dehydrogenase (LDH). A possible explanation for the elevation of lactate in the supernatant of co-culture compared with the associated *E. coli* monocultures may be due to production of lactate by Caco-2 cells (Fig. 3). The remaining pyruvate from aerobic glycolysis enters the TCA cycle in the mitochondrion. Notably, lactate may not only be utilized for oxidation or energetic purposes, but also act as a growth or survival signal in the wound healing process, allowing the production of growth factors and cytokines[37]. Lactate accumulation is a sign of a wound regardless of oxygen concentration, thus enhancing the immune response to infection and potentially increasing cellular response to repair the lesion with an increased immune response[38]. Furthermore, the antiporter-based malate-aspartate shuttle regenerates NAD^+ in the cytosol to regulate the glycolytic flux[39]. We speculate that in co-culture, depletion of aspartate impairs the regulation of NAD^+/NADH balance, and as a result favors the production of NAD^+ via LDH. Accumulated intracellular BCAAs can further direct pyruvate to the TCA cycle or lactate biosynthesis. However, insufficient succinate dehydrogenase could disrupt the TCA cycle and push metabolic efflux away from mitochondria in favor of lactate and NAD^+ production (Fig. 6). Notably, while Caco-2 cells have been used as a well-established model in studying metabolic crosstalk between pathogens and

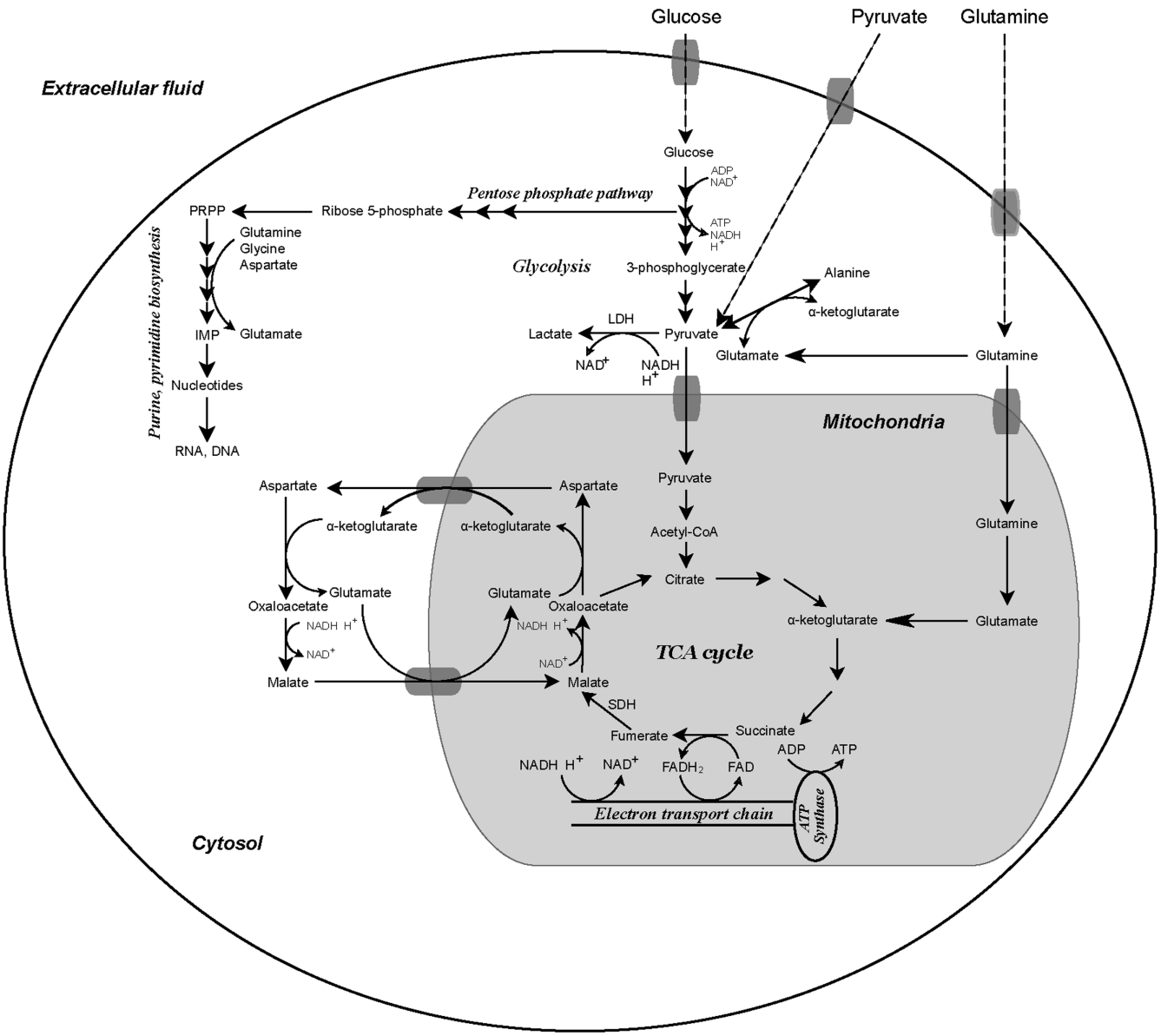

Figure 6 | A schematic pathway illustrating the significant metabolic changes of Caco-2 cells induced by *E. coli*. In the condition of low glucose and glutamine uptake, the metabolic efflux is altered in order to maintain the function of the mitochondrial shuttle system and generate NAD^+ in the cytosol.

human cells, it remains to be explored whether Caco-2 cells are behaving more cancer-like or normal while interacting with microbes in vitro. Nevertheless, the increased SOD in the gene expression profile can serve as a protective agent that substantially delays free radical overproduction and initiate host defense mechanisms for oxidative stress and activation of inflammation. The excess ROS induces mitochondrial dysfunction and inactivates the electron transport chain and/or ATP synthase which may also explain why there is an alteration in the intracellular succinate/fumarate ratio.

Significant oxidative stress as well as coupled pro-inflammatory responses induced by intestinal microbiota is likely an important cause of a variety of GI diseases including IBD and colorectal cancer[40–42]. The damaged intestinal epithelial barrier usually introduces bacterial infection in the normally sterile submucosal layer, triggering a cascade of immune responses[40–42]. We characterized and compared the dynamics of the transcriptional and metabolic response of a human colon adenocarcinoma-derived cell line cultured with one of two strains of *E. coli* at the molecular and cellular level. Importantly, our results support the hypothesis that intestinal microbiota are responsible for the alteration of host metabolic activity. Our finding will lead to a deeper understanding of the bacterial-host interaction and the potential effect of this relationship on diet, stress, inflammation and infection.

Methods

Cell culture. *E. coli culture.* *E. coli* K-12 and *E. coli* O157:H7 were obtained from the American Type Culture Collection (ATCC 10798 and 35150, Manassas, VA) and grown under aerobic conditions in trypticase soy broth media (Becton Dickinson, Sparks, MD) in an incubator-shaker at 37°C. For all experiments, *E. coli* cultures were grown overnight and used in the early stationary phase.

Caco-2 cell culture. The human colon adenocarcinoma cell line Caco-2 (passages 26–30), obtained from ATCC was grown at 37°C and 5% CO_2 in a humidified atmosphere in 75 cm^2 flasks with Dulbecco's modified Eagle's essential medium (DMEM) containing high glucose and supplemented with 2 mM L-glutamine (in the form of l-alanyl-l-glutamine dipeptides, GlutaMAX™ supplement, Life Technologies, catalog number 35050061), 1 mM sodium pyruvate, 16.6% fetal bovine serum (FBS) v/v, 10 IU/mL penicillin, 0.10 mg/mL streptomycin and 1X non-essential amino acids in accordance with ATCC recommendations. Due to the fact that these cells were co-cultured with bacterial cells an additional buffer composed of 10 mM 3-morpholinopropanesulfonic acid (MOPS), 10 mM N-(Tris(hydroxymethyl)methyl) -2-aminoethanesulfonic acid (TES), 15 mM 4-(2-hydroxyethyl)-1-piperazineethanesulfonic acid (HEPES), and 2 mM sodium phosphate was added to further buffer the

media (pH 7.2). Media was changed every 2–3 d. All assays were using differentiated Caco-2 (typically 21–22 d post inoculation).

Caco2-E. coli Co-culture. 24 hours prior to inoculation with *E. coli*, complete media was changed to media lacking antibiotics and serum. Caco-2 cells were subsequently infected with bacteria at a multiplicity of infection (MOI) of 1,000 in 10 mL of cell culture media lacking antibiotics and serum. Controls included flasks with Caco-2 or bacterial cells alone. Flasks with Caco-2 cells alone and with co-culture were centrifuged at low speed (~164 rcf) for 5 minutes to ensure bacterial adherence with the monolayer. To determine the metabolic responses of Caco-2 upon interaction with *E. coli* K-12, comparisons between Caco-2 controls (n = 6), *E. coli* K-12 controls (n = 6) and the Caco2-*E. coli* co-cultures (n = 6) were performed at 60 minutes. To explore the dynamic interaction effect between Caco-2 cells and one of two strains of *E. coli* on both gene expression pattern and extracellular metabolic profiles, a time series observations between Caco-2 controls (n = 2), *E. coli* K-12 controls (n = 2), *E. coli* O157:H7 controls (n = 2) and Caco-2-*E. coli* K-12 cocultures (n = 2) and Caco-2-*E.coli* O157:H7 cocultures (n = 2) were performed at 60, 90 and 120 minutes.

Prior to the experiment, cell culture media was collected (n = 4) to determine the metabolic baseline. At the desired time points (60, 90, and 120 minutes), supernatant (containing media with or without bacteria) was collected, centrifuged at 10,000 × g for 5 min at 4°C to remove cell debris and bacteria, and stored at −80°C. Subsequently, 10 mL aliquots of Trizol LS (Invitrogen, Carlsbad, CA) were added to the flasks with Caco-2 cells (control or co-culture) or to the tubes containing control bacterial pellets. Cells were lysed by repeated pipetting in Trizol LS. All samples were stored at −80°C until RNA extraction.

To determine the impact of *E. coli* K-12 on Caco-2 intracellular metabolic profile, Caco-2 cells were incubated with *E. coli* K-12 for 60 minutes (n = 3) and compared with the Caco-2 controls (n = 3). To harvest mammalian cells for intracellular metabolite analysis, cells were washed several times with ice-cold phosphate buffered saline (PBS), and collected from the flasks in 10 mL of PBS using cell scrapers. Cells were pelleted by centrifugation (400 × g for 10 min at 4°C), frozen on dry ice, and stored at −80°C until extraction. Intracellular metabolites were extracted using a methanol/chloroform extraction procedure[43], lyophilized for 48 hours with Labconco FreeZone 4.5L Benchtop FreezeDry system (Labconco, Kansas City, MO), and stored at −80°C for later analysis.

Gene expression analysis. *Preparation of RNA.* Samples of Caco-2 cells in Trizol were freeze-thawed three times in order to improve host cell lysis. Co-culture samples were centrifuged (10,000 × g for 5 min) to pellet any remaining *E. coli* cells. The supernatant was used to extract total Caco-2 RNA according to the manufacturer's protocol (Invitrogen, Carlsbad, CA). Total RNA extracted from Caco-2 cells was further purified using RNeasy Mini Kit (Qiagen, Valencia, CA). RNA yield was quantified by UV absorbance at 260 and 280 nm with a Nanodrop system (Thermo Scientific, Wilmington, DE). RNA quality was assessed using a Bioanalyzer (Agilent Technologies, Santa Clara, CA).

Starting with 500 ng of total Caco-2 RNA for each sample, double-stranded cDNA was synthesized and biotinylated aRNA was generated using GeneChip 3′ IVT Express Kit (Affymetrix, Fremont, CA). GeneChip Sample Cleanup Module (Affymetrix) was used to clean up aRNA according to the manufacturer's protocol. For the final fragmentation of labeled aRNA, GeneChip 3′ IVT Express Kit was used. 15 ug in 40 μL of fragmented and labeled aRNA from Caco-2 samples were prepared for hybridization on the GeneChip Human Genome U133 Plus 2.0 Arrays (Affymetrix).

Fragmented and labeled Caco-2 aRNA samples with corresponding GeneChips were submitted for hybridization and scan to UC Davis School of Medicine Microarray Core Facility equipped with Fluidics Station 450, Hybridization oven 640, and 3,000 GeneChip Scanner with Autoloader (Affymetrix) and were processed according to Affymetrix protocols.

Microarray analysis. Data were preprocessed using affy package from BioConductor[44]. The signal channel array data were normalized and background corrected expression values were created using the robust multi-array average (RMA) method[45]. Differentially expressed genes at each time point were computed using an Excel add-in application, Significance Analysis of Microarrays (SAM) v3.11[46].

All human differentially expressed genes were imported into Ingenuity Pathways Analysis (IPA) program (Ingenuity Systems, Mountain View, CA) for biological function annotation. The human Genome Affymetrix array knowledge base was selected with a filtering setting of all colon cancer cell lines. Gene expression profile data are accessible as MIAME format on the NCBI Gene Expression Omnibus (GEO) website (http://www.ncbi.nlm.nih.gov/geo/), with accession number GSE50040. Two biological replicate experiments were done for each time point.

^{1}H NMR metabolomics analysis. Supernatant samples were thawed and filtered through 3,000 MW cutoff filters (Pall, Ann Arbor, MI) to remove lipids and proteins. Lyophilized cell extract samples were reconstituted in 280 μL of Type I ultrapure water from a Millipore Synergy UV system (Millipore, Billerica, MI), and centrifuged at 14,000 × g for 10 min at 4°C to pellet debris.

Samples were prepared for NMR analysis by the addition of 65 μL of the internal standard DSS-d6 (2,2,3,3,4,4-d6-3-(trimethylsilyl)-1-propane sulfonic acid) (at 5 mM) to 585 μL of filtered supernatant, or 23 μL of DSS-d6 to 207 μL cell extracts dissolved in Type I H_2O, and the pH was adjusted to approximately 6.8 by the addition of small amounts of NaOH or HCl. 600 μL or 180 μL of NMR samples were placed into 5 mm or 3 mm NMR tubes respectively (Bruker Biospin Corporation, Billerica, MA). NMR spectra were acquired at 25°C on a Bruker 600 MHz NMR spectrometer equipped with a SampleJet using the Bruker "noesypr1d" pulse sequence. Acquisition parameters were: 12 ppm sweepwidth, 2.5 s acquisition time, 2.5 s relaxation delay, 100 ms mixing time, 8 dummy scans, and 32 transients for supernatants or 1,600 for cell extracts. Water suppression was applied during the 2.5 s relaxation delay and the 100 ms mixing time. All spectra were zero-filled to 128k data points, and a weighted Fourier Transform with 0.5 Hz of line-broadening was applied with manual phase and baseline correction. Analysis of the NMR data was accomplished through targeted profiling using Chenomx NMRSuite v6.1 (Chenomx Inc., Edmonton, Canada)[47].

Statistical analysis. A gene was considered differentially expressed between a test condition and a control using a threshold of 1.2 fold change and 5% false discovery rate (FDR). For metabolomics experiments, $\log_{10}$ transformation was applied to approximate normal distribution. Two-tailed, two-sample Student's t-test was applied to assess the change of intracellular pH between the Caco-2 control and the Caco2-*E. coli* K-12 coculture. For each measured metabolite, repeated measures ANOVA was applied to examine the overall effect over time. After FDR correction, p-value < 0.05 was considered statistically significant. For multivariate analysis, Principal Component Analysis (PCA) was performed using SIMCA-P+ (version 13; Umetrics, Umeå, Sweden). All metabolomics data are expressed as mean ± SEM.

1. Cucchiara, S., Iebba, V., Conte, M. P. & Schippa, S. The microbiota in inflammatory bowel disease in different age groups. *Dig. Dis.* **27**, 252–258 (2009).
2. Tiihonen, K., Ouwehand, A. C. & Rautonen, N. Human intestinal microbiota and healthy ageing. *Ageing. Res. Rev.* **9**, 107–116 (2010).
3. Wu, G. *et al.* Linking long-term dietary patterns with gut microbial enterotypes. *Science.* **334**, 105–108 (2011).
4. He, X., Marco, M. & Slupsky, C. Emerging Aspects of Food and Nutrition on Gut Microbiota. *J. Agric. Food Chem. DOI: 10.1021/jf4029046* (2013).
5. Musso, G., Gambino, R. & Cassader, M. Interactions between gut microbiota and host metabolism predisposing to obesity and diabetes. *Annu. Rev. Med.* **62**, 361–380 (2011).
6. Tilg, H. & Kaser, A. Gut microbiome, obesity, and metabolic dysfunction. *J. Clin. Invest.* **121**, 2126–2132 (2011).
7. Turnbaugh, P. & Gordon, J. The core gut microbiome, energy balance and obesity. *J. Physiol.* **587**, 4153–4158 (2009).
8. Martin, F. P. J. *et al.* A top-down systems biology view of microbiome-mammalian metabolic interactions in a mouse model. *Mol. Syst. Biol.* **3**, 112 (2007).
9. Cummings, J. H. & Macfarlane, G. T. Role of intestinal bacteria in nutrient metabolism. *JPEN J. Parenter. Enteral. Nutr.* **21**, 357–365 (1997).
10. Holmes, E., Li, J., Athanasiou, T., Ashrafian, H. & Nicholson, J. Understanding the role of gut microbiome-host metabolic signal disruption in health and disease. *Trend. Microbiol.* **19**, 349–359 (2011).
11. Cani, P. & Delzenne, N. The gut microbiome as therapeutic target. *Pharmacol. Ther.* **130**, 202–212 (2011).
12. Fanaro, S., Chierici, R., Guerrini, P. & Vigi, V. Intestinal microflora in early infancy: composition and development. *Acta. Paediatr. Suppl.* **91**, 48–55 (2003).
13. Vajro, P., Paolella, G. & Fasano, A. Microbiota and gut-liver axis: their influences on obesity and obesity-related liver disease. *J. Pediatr. Gastroenterol. Nutr.* **56**, 461–468 (2013).
14. Barnich, N. *et al.* CEACAM6 acts as a receptor for adherent-invasive E. coli, supporting ileal mucosa colonization in Crohn disease. *J. Clin. Invest.* **117**, 1566–1574 (2007).
15. Rolhion, N. & Darfeuille-Michaud, A. Adherent-invasive Escherichia coli in inflammatory bowel disease. *Inflamm. Bowel Dis.* **13**, 1277–1283 (2007).
16. Barnich, N. & Darfeuille-Michaud, A. Adherent-invasive Escherichia coli and Crohn's disease. *Curr. Opin. Gastroenterol.* **23**, 16–20 (2007).
17. Bronowski, C. *et al.* A subset of mucosa-associated Escherichia coli isolates from patients with colon cancer, but not Crohn's disease, share pathogenicity islands with urinary pathogenic E. coli. *Microbiology.* **154**, 571–583 (2008).
18. Santacruz, A. *et al.* Interplay between weight loss and gut microbiota composition in overweight adolescents. *Obesity (Silver Spring).* **17**, 1906–1915 (2009).
19. Santacruz, A. *et al.* Gut microbiota composition is associated with body weight, weight gain and biochemical parameters in pregnant women. *Br. J. Nutr.* **104**, 83–92 (2010).
20. Tedelind, S., Westberg, F., Kjerrulf, M. & Vidal, A. Anti-inflammatory properties of the short-chain fatty acids acetate and propionate: a study with relevance to inflammatory bowel disease. *World J Gastroenterol* **13**, 2826–2832 (2007).
21. Chang, L. & Karin, M. Mammalian MAP kinase signalling cascades. *Nature.* **410**, 37–40 (2001).
22. Chen, Z. *et al.* Induction and superinduction of growth arrest and DNA damage gene 45 (GADD45) alpha and beta messenger RNAs by histone deacetylase inhibitors trichostatin A (TSA) and butyrate in SW620 human colon carcinoma cells. *Cancer Lett.* **188**, 127–140 (2002).
23. Hernandez-Saavedra, D., Zhou, H. & McCord, J. M. Anti-inflammatory properties of a chimeric recombinant superoxide dismutase: SOD2/3. *Biomed. Pharmacother.* **59**, 204–208 (2005).

24. Sydora, B. *et al*. An imbalance in mucosal cytokine profile causes transient intestinal inflammation following an animal's first exposure to faecal bacteria and antigens. *Clin. Exp. Immunol.* **161**, 187–196 (2010).
25. Fukushima, K. *et al*. Non-pathogenic bacteria modulate colonic epithelial gene expression in germ-free mice. *Scand. J. Gastroenterol.* **38**, 626–634 (2003).
26. Jarvis, K. *et al*. Enteropathogenic Escherichia coli contains a putative type III secretion system necessary for the export of proteins involved in attaching and effacing lesion formation. *Proc. Natl. Acad. Sci. U. S. A.* **92**, 7996–8000 (1995).
27. Nataro, J. P. & Kaper, J. B. Diarrheagenic escherichia coli. *Clin. Microbiol. Rev.* **11**, 142–201 (1998).
28. Wolfe, A. The acetate switch. *Microbiol. Mol. Biol. Rev.* **69**, 12–50 (2005).
29. Alam, K. & Clark, D. Anaerobic fermentation balance of Escherichia coli as observed by in vivo nuclear magnetic resonance spectroscopy. *J. Bacteriol.* **171**, 6213–6217 (1989).
30. Ganesan, B. & Weimer, B. C. Role of aminotransferase IlvE in production of branched-chain fatty acids by Lactococcus lactis subsp. lactis. *Appl. Environ. Microbiol.* **70**, 638–641 (2004).
31. Ganesan, B., Stuart, M. R. & Weimer, B. C. Carbohydrate starvation causes a metabolically active but nonculturable state in Lactococcus lactis. *Appl. Environ. Microbiol.* **73**, 2498–2512 (2007).
32. Ganesan, B., Seefeldt, K. & Weimer, B. C. Fatty acid production from amino acids and alpha-keto acids by Brevibacterium linens BL2. *Appl. Environ. Microbiol.* **70**, 6385–6393 (2004).
33. Ganesan, B., Seefeldt, K., Koka, R. C., Dias, B. & Weimer, B. C. Monocarboxylic acid production by lactococci and lactobacilli. *Int. Dairy J.* **14**, 237–246 (2004).
34. Ganesan, B., Dobrowolski, P. & Weimer, B. C. Identification of the leucine-to-2-methylbutyric acid catabolic pathway of Lactococcus lactis. *Appl. Environ. Microbiol.* **72**, 4264–4273 (2006).
35. Reeds, P. J. & Burrin, D. G. Glutamine and the bowel. *J. Nutr.* **131**, 2505S–2508S; discussion 2523S–2504S (2001).
36. Brand, K. & Hermfisse, U. Aerobic glycolysis by proliferating cells: a protective strategy against reactive oxygen species. *FASEB J.* **11**, 388–395 (1997).
37. Kennedy, K. M. & Dewhirst, M. W. Tumor metabolism of lactate: the influence and therapeutic potential for MCT and CD147 regulation. *Future Oncol.* **6**, 127–148 (2010).
38. Trabold, O. *et al*. Lactate and oxygen constitute a fundamental regulatory mechanism in wound healing. *Wound Repair Regen.* **11**, 504–509 (2003).
39. Dawson, A. G. Oxidation of cytosolic NADH formed during aerobic metabolism in mammalian cells. *Trends. Biochem. Sci.* **4**, 171–176 (1979).
40. Naik, E. & Dixit, V. M. Mitochondrial reactive oxygen species drive proinflammatory cytokine production. *J. Exp. Med.* **208**, 417–420 (2011).
41. Rezaie, A., Parker, R. D. & Abdollahi, M. Oxidative stress and pathogenesis of inflammatory bowel disease: an epiphenomenon or the cause? *Dig. Dis. Sci.* **52** (2007).
42. Ullman, T. A. & Itzkowitz, S. H. Intestinal inflammation and cancer. *Gastroenterology.* **140**, 1807–1816 (2011).
43. McGrath, B. M., Greenshaw, A. J., McKay, R., Slupsky, C. M. & Silverstone, P. H. Lithium alters regional rat brain myo-inositol at 2 and 4 weeks: an ex-vivo magnetic resonance spectroscopy study at 18.8 T. *Neuroreport.* **17**, 1323–1326 (2006).
44. Gentleman, R. C. *et al*. Bioconductor: open software development for computational biology and bioinformatics. *Genome. Biol.* **5**, R80 (2004).
45. Irizarry, R. A. *et al*. Summaries of Affymetrix GeneChip probe level data. *Nucleic. Acids. Res.* **31**, e15 (2003).
46. Tusher, V. G., Tibshirani, R. & Chu, G. Significance analysis of microarrays applied to the ionizing radiation response. *Proc. Natl. Acad. Sci. U. S. A.* **98**, 5116–5121 (2001).
47. Weljie, A. M., Newton, J., Mercier, P., Carlson, E. & Slupsky, C. M. Targeted profiling: quantitative analysis of 1H NMR metabolomics data. *Anal. Chem.* **78**, 4430–4442 (2006).

Acknowledgments

We are particularly grateful to Dr. Alline Pacheco, Dr. Aifric O'Sullivan, Dr. Ann Spevacek, Elizabeth Chin and Jennie Sotelo for helpful discussion and comments. We thank Xinran Dong for help and advice on microarray data analysis.

Author contributions

X.H. and C.S. interpreted the data. X.H. prepared figures and wrote the manuscript. D.M. and J.S. performed the experiment. X.H., D.M. and C.S. analyzed the data. B.W. and C.S. designed the experiment. C.S. edited the manuscript and supervised the project. All authors discussed the result and reviewed the manuscript.

Additional information

Accession codes: the GEO submission accession number is GSE50040

Supplementary information accompanies this paper at http://www.nature.com/scientificreports

Competing financial interests: The authors declare no competing financial interests.

How to cite this article: He, X., Mishchuk, D.O., Shah, J., Weimer, B.C. & Slupsky, C.M. Cross-talk between *E. coli* strains and a human colorectal adenocarcinoma-derived cell line. *Sci. Rep.* **3**, 3416; DOI:10.1038/srep03416 (2013).